IAC-14-A6.9.4

Orbit Determination of Space Debris Using a Bi-static Radar Configuration with a Multiple-Beam Receiver

Alessandro Morselli
Dipartimento di Scienze e Tecnologie Aerospaziali, Politecnico di Milano, Italy
alessandro.morselli@polimi.it

Roberto Armellin
School of Engineering Sciences, University of Southampton, UK
roberto.armellin@soton.ac.uk

Pierluigi Di Lizia, Franco Bernelli Zazzera
Dipartimento di Scienze e Tecnologie Aerospaziali, Politecnico di Milano, Italy
{ pierluigi.dilizia, franco.bernelli }@polimi.it

Emma Salerno, Germano Bianchi, Stelio Montebugnoli
Istituto di Radioastronomia, Istituto Nazionale di Astrofisica, Bologna, Italy
{ esalerno, g.bianchi, s.montebugnoli }@ira.inaf.it

Alessio Magro
Department of Physics, University of Malta, Malta
alessio.magro@um.edu.mt

Kristian Zarb Adami
Astrophysics, Department of Physics, University of Oxford, United Kingdom
kristian.zarbadami@astro.ox.ac.uk

Abstract

In this work the use of a multi-beaming radar system is analyzed and a possible setup of a closed loop system (i.e. from measurement and data acquisition to orbit determination) is described. The Orbit Determination (OD) algorithms are specialized for a bistatic radar configuration where the Medicina Northern Cross radio-telescope (owned by the University of Bologna - Italy) is considered as a receiver. The Northern Cross is composed of two perpendicular arms: the E/W arm is 564 m long and consists in a single cylindrical antenna with a width of 29.4 m, whereas the N/S arm is made of 64 parallel antennas with a length of 22.6 m and a width of 7.5 m. The collecting area reaches 27,400 sqm and, by considering a complete upgrade of the radar with the installation of new receivers on the focal lines, up to 22,880 possible theoretical independent beams could cover the field-of-view of 55.47 (E/W) deg x 1.8 (N/S) deg. By looking at the sequence of beams that are illuminated, it is thus possible to estimate, with an higher level of detail with respect to the single-beam system, the ground track of the transiting object.

Given this peculiar system, tailored orbit determination algorithms have to be developed. The orbit determination algorithm receives as input the data processed by the acquisition system, that digitally assembles measured radar echoes, using Fast Fourier Transform, to provide the signal for each beam. These inputs are the measured Doppler shift, time delay, the illumination time and measured power intensity associated to each beam. By combining these information with the knowledge of beam distribution and pointing it is possible to refine the orbital parameters of known objects or to perform a preliminary OD.

A few LEO objects are considered to generate simulated data that are then used to feed the developed OD algorithms. In this way the performances of the algorithms can be tested and the effectiveness of this innovative configuration for space debris measurements, that couples a bistatic radar and a multi-beaming receiver, can be assessed.

I INTRODUCTION

The number of manmade objects orbiting the Earth has dramatically increased during the last decades, posing a serious risk for space based activities. Most of the objects currently orbiting the Earth are classified as "space debris", that comprise inactive satellites, discarded launch

stages, and fragments originated from satellite breakups and collisions. Several counter measures have been adopted with the aim of reducing mission related risks and casualties (e.g. orbital collisions) and to control the number of objects in orbit. Disposal and mitigation strategies are now taken into account during the mission design and collision risk assessment is performed on a daily basis by satellite operators. Conjunction Summary messages are provided to satellite operator by USSTRATCOM to support decisions on the execution of collision avoidance maneuvers (1). An accurate estimation of objects trajectory is also required to estimate on ground risk from satellite or debris re-entry. As a consequence, the characterization of the orbital environment plays a crucial role since it provides the data required both in the mission design phase (debris population models) and risk assessment (estimation of debris trajectory).

Survey and tracking of objects in Earth orbit is one of the main areas where the ESA Space Situational Awareness (SSA) programme is active. The objective of the SSA initiative is to support the European independent utilization of and access to space through the provision of timely and accurate information and data regarding the space environment, and particularly regarding hazards to infrastructure in orbit and on the ground. To meet this requirement, the implementation of a European network of sensors for surveillance and tracking of objects in Earth's orbit is mandatory. Besides the implementation of newly developed infrastructure including optical survey telescopes, new test radars and dedicated future satellite missions, the SSA programme also considers the use of existing European national assets in the future space surveillance and space situational awareness system. In the light of this, the Italian Northern Cross radio telescope array was selected as a possible component of the SSA network, due to its large collecting area (∼27,000 sqm) and its position in the center of the European territory. The Northern Cross (Fig. 1) is located at the Medicina Radioastronomical Station, close to Bologna, in northern Italy. It is owned by the University of Bologna but managed and operated by the Istituto di Radioastronomia of the Istituto Nazionale di Astrofisica (INAF-IRA).

Figure 1: A top view of the Medicina Radioastronomical Station. In the foreground the Northern Cross T-shaped array.

In the framework of the SSA Preparatory Program (SSA-PP), the INAF-IRA developed and executed a work plan under the Statement of Work "Medicina Support Activities for Surveillance Validation and Operations", with the purpose of checking the suitability of the Northern Cross to participate in the SSA program. In particular, UHF-band measurements were carried out in order to test the Northern Cross as receiving part of bi- or multi-static radar systems for space debris monitoring at different orbital regions.

Further developments in the postprocessing phase were carried out in collaboration with the University of Malta. A digital backend that allows the beamforming of 32 beams distributed across the receiver field of view was implemented and tested.

The developed system requires tailored algorithms for orbit determination due to the presence of a multi-beaming receivers in a bistatic radar asset. In this paper the algorithms developed by the group of the Politecnico di Milano are described and some preliminary results are given.

II RADAR OBSERVATIONS OF SPACE DEBRIS

Space debris observing campaigns mainly employ radars and optical sensors to detect, identify, and maintain tracks for both known and uncatalogued fragments. While optical observations reach very good performances in Geostationary Earth Orbit (GEO) and in the Geostationary Transfer Orbit (GTO), radar techniques outperform optical facilities in LEO. Ground-based radars provide a powerful tool for the characterization of the orbital debris environment (2). Radars can in fact irradiate at any time a satellite or space debris in Earth orbit with a microwave beam. The scattered wave is detected by a receiver that may be the same transmitting antenna (monostatic radar) or a different one located at a distance of up to several hundreds of kilometers away (bistatic radar). When more than two antennas with common spatial coverage are employed and data from each site is combined at a central location, the system is called a multistatic radar.

Due to the high sensitivity and the capability to operate independently of the weather, day-night conditions and illumination of the target by sunlight, radar observations have been used to statistically sample the population of space debris in Earth orbit down to a few centimeters in size (3, 4). Position, time of detection and reflected energy of the detected objects, computed as Radar Cross Section (RCS), are some of the important information that can be derived from radar measurements (5).

The scenario considered in this work takes into account the beam park observation technique. With this method the transmitting and the receiving antennas stares along a fixed direction and the receiver detects echoes coming from space debris that transits through the common field of view. The beam park method can be utilized to detect both known and uncatalogued fragments at any altitude, provided that the reflected power captured by the receiver is distinguishable from the noise.

II.I The Radar Components

Two different bistatic systems are considered, with two different transmitters and the Northern cross always playing the role of receiver. The first configuration is between a monostatic and a bistatic radar system since the transmitting antenna is located at approximately 20 km from the receiver (we can define this configuration "quasi-monostatic"), whereas the second configuration is a pure bistatic radar system with a transmitter located in Sardinia, Italy. The main characteristics of the three antennas are summarized in Tab. 1. More details on each antenna are given in the following subsections.

The Northern Cross

The Northern Cross radio telescope is a T-shaped array that was designed and built during 60's. It operates at UHF-band (408 MHz) with a bandwidth from approximately 2.5 MHz (old part) up to 16 MHz (upgraded part). It is a transit instrument, steerable in declination only, and therefore able to point at objects that transit over the local celestial meridian. The radio telescope is composed of two perpendicular branches (see Fig. 2): the first arm is aligned in an E-W direction and the second one in a N-S direction.

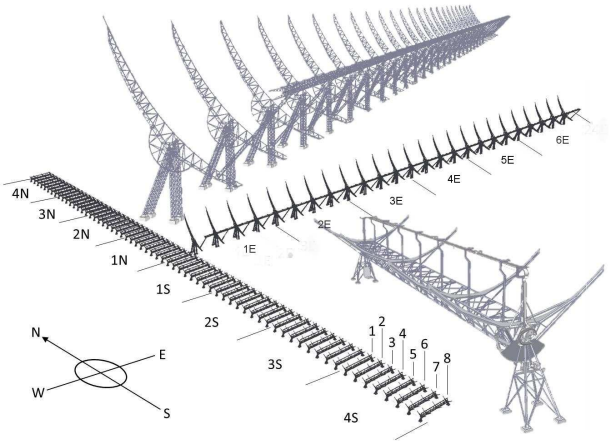

Figure 2: A scheme of the Northern Cross antenna divided by channels. In the foreground and in the background, in gray, a detailed drown of one antenna of the N-S arm and of the whole E-W arm, respectively.

Table 1: Main features of the antennas composing the ground-based radar system for space debris monitoring - col. 1: antenna name; col. 2, 3, 4: geographical coordinates of the antennas; col. 5: antenna size (for the Northern Cross, given value corresponds to the equivalent circular diameter); col. 6: central frequency; col. 7: radar component (Tx = transmitter, Rx = receiver); col. 8: signal wave polarization; col. 9, 10: antenna's pointing limits.

Antenna	Latitude	Longitude	Altitude	Diameter	Band	Comp.	Polarization	Azimuth	Elevation
Northern Cross	44°31'14"N	11°38'49"E	25 m	185 m	UHF	Rx	Linear (HLP)	0,180 deg	>45deg
Bagnara	44°23'56"N	11°51'15"E	18 m	3 m	UHF	Tx	Linear (HLP)	50-200 deg	>20 deg
SRT	39°29'35"N	09°14'43"E	650 m	7 m	UHF	Tx	Linear (HLP)	0-360 deg	>20 deg

The E-W branch is a unique antenna with a 564 m long and 29.4 m wide cylindrical-parabolic reflector surface (geometrical collecting area of 16,600 sqm). It is supplied with 1536 dipoles that lie out along the focal axes and transform the incident radio waves to measurable voltages. The N-S arm is composed of 64 parallel cylindrical-parabolic shaped antennas. Each antenna is 22.6 m long and 7.5 m wide and it is set at a distance of 10 m from the next one (total geometrical collecting area of 10,800 sqm). Currently, each antenna is equipped with 64 dipoles for a total of 4096 receivers for the whole N-S arm. The cylindrical-parabolic shape of the Northern Cross reflectors allows the incoming radiation to converge on the antenna's focus and to keep the phase unmodified after its reflection. The reflector is composed of a number of steel wires aligned at a distance of approximately 2 cm from each other.

At the typical observing wavelengths (73.5 cm), the mechanical precision of this structure results sufficient to guarantee unaltered the instrument performances.

With its 27,400 square metres of total collecting area the Northern Cross represents the largest UHF-capable antenna in the Northern hemisphere, with an aperture efficiency of 60%, second only to Arecibo in the world wide scale. Such a wide area potentially allows the constant monitoring of a large number of space debris. Numerical simulations were performed by our group to determine the maximum number of orbiting objects that pass into the Northern Cross Field of View (FOV) as a function of the total number of feeds installed on the two arms. The simulations showed a capability to detect 85% of the NORAD catalogued objects.

The transmitters

Two configurations are considered. The first one takes into account a transmitter located close to the Northern Cross whereas the second one a transmitting antenna located in Sardinia, Italy.

Figure 3: The 3-mt dish transportable antenna

For the first transmitter, a 3-mt diameter antenna, developed and manifactured by ESSAT (an Italian company leader, at national level, in designing and manufacturing antennas and antenna systems for telecommunication applications) is taken into account. The antenna, a transportable parabolic dish (Fig. 3), is equipped with a set of Tx modules that were installed on the feed to allow transmission powers up to 1 kW. A dummy load was also mounted on the feed to grant an instantaneous on-off switching of the transmission, without time delay for the power to reach its maximum level. This artifice allowed a considerable improvement of the trans-

mitting timing. The location of the antenna is at approximately 20 km from the Northern Cross. A set of tests was performed, including the utilization of different types of Tx feeds (dual linear polarization feed and linear polarized dipole feed), in order to investigate their suitability for the Northern Cross receiving system. The evaluation and trade off of the different performance efficiencies brought to the conclusion that dual linear polarization dipole feeds were preferable to increase the entire sensitivity levels of the radar system.

The second transmitter is an hypotetical 7-mt diameter antenna, located close to Sardinia Radio Telescope (SRT), near San Basilio (Cagliari, Italy). The same manufacturing characteristics are considered for this antenna. In this case the maximum transmitting power is supposed equal to 5 kW.

II.II Backend

The 32 analog signals from the BEST-2 array (6) are fed to a ROACH-based digital backend developed by (7), where they are digitised and channelized into a total of 1024 single-polarisation, coarse frequency channels. The digital backend processes 20 MHz of bandwidth, even though only 16 MHz are useful. The channelized data is then encapsulated as a UDP stream and is sent to a compute server over a 10 GbE link, which hosts an NVIDIA Tesla K20 GPU that is used to beamform and finely channelize the data stream. The real-time GPU pipeline from (8) was used as a base for the space debris pipeline. The UDP stream is received, interpreted and buffered by a high-speed packet receiver which copies the data to GPU memory. An optimised, GPU-based multi-beam beamformer generates 32 beams distributed across the array's primary FoV. Each beam is then further channelized to a spatial resolution of 38.15 Hz (1024 channels per coarse subband). A subset of the fine channels from each beam are then copied back to host memory and saved to a file for offline processing.

The following steps are executed during offline processing:

- Calculate the bandpass in each beam and pass it through a median filter
- Subtract the bandpass from the data, thus removing noisy RFI channels without affecting any transit
- Normalise and threshold the data to remove background noise
- Apply a Hough transform to produce a series of lines present in the data, which should correspond to transits
- For each time step, increment a counter associated with the beam which contains the most power to generate a multi-pixel plot

III BISTATIC RADAR SIMULATOR

A simulator of the bistatic radar configuration described above was developed to support analysis and estimate the system performances, that has also the capability of generating data resembling those that could be measured in reality. The simulator is designed so that different kind of transmitter and multibeam geometry can be easily defined by the user.

A sketch of the geometric configuration of the bistatic radar system is given in Figure 4. A plane that contains the two relative distance vectors from Tx and Rx, ρ_{Tx} and ρ_{Rx} respectively, and the baseline L can be defined. This plane is usually indicated as bistatic plane and it allows for easy computations of all range relationships.

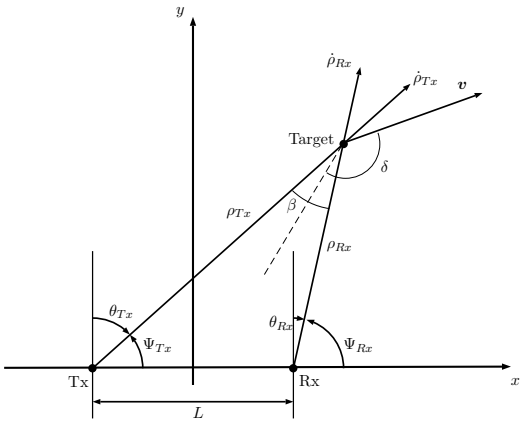

Figure 4: Geometry of the radar system on the bistatic plane.

Given the trajectory of an object (e.g. computed using SGP4/SDP4 and available TLE) the range from Tx and Rx, ρ_{Tx} and ρ_{Rx} respectively, are directly computed using the positions of the two antennas. The time interval ΔT between the transmission of the pulse and the reception of the target echo is obtained from

$$\rho_{Tx} + \rho_{Rx} = c\Delta T, \quad [1]$$

where c is the speed of light.

The bistatic doppler shift, when ignoring relativistics effects, is computed as

$$\Delta f = \frac{1}{\lambda}\left(\dot{\rho}_{Tx} + \dot{\rho}_{Rx}\right), \quad [2]$$

where λ is the wavelength of the transmitted signal and $\dot{\rho}_{Tx}$ and $\dot{\rho}_{Rx}$ are the projections of the target velocity onto the transmitter-to-target and receiver-to-target line of sight (LOS). When both Tx and Rx are stationary the Doppler shift becomes

$$\Delta f = \frac{2V}{\lambda}\cos\delta\cos\left(\frac{\beta}{2}\right). \quad [3]$$

In our case, we transformed satellite position and velocity into ECEF (Earth-centered Earth-fixed frame) so that the velocity of Tx and Rx are zero and then projected the ECEF velocity of the satellite $\boldsymbol{v}$ on the range vectors direction, obtaining

$$\Delta f = \frac{1}{\lambda}\left(\boldsymbol{v}\cdot\hat{\boldsymbol{\rho}}_{Tx} + \boldsymbol{v}\cdot\hat{\boldsymbol{\rho}}_{Rx}\right). \quad [4]$$

For each beam of Rx is then possible to compute the received power using the bistatic radar equation

$$P_{Rx} = \frac{P_{Tx}\,G_{Tx}\,G_{Rx}\,\lambda^2\,\sigma_b}{(4\pi)^3\,\rho_{Tx}^2\rho_{Rx}^2}, \quad [5]$$

where P_{Tx} is the transmitter power, G_{Tx} and G_{Rx} are the antenna gains, and σ_b is the radar cross section. The information on the satellite radar cross section were downloaded from Space-Track*. At each time step the ranges ρ_{Tx} and ρ_{Rx} are obtained from orbit propagation and the antenna gains are updated using an elliptical model for the beam, expressed by

$$G_{dB} = G_{dB0} - 12\left(\left(\frac{\Delta\alpha}{BW_\alpha}\right)^2 + \left(\frac{\Delta\delta}{BW_\delta}\right)^2\right), \quad [6]$$

where $G_dB = 10\log_{10}G$, G_{dB0} is the reference gain of the antenna in decibel, $\Delta\alpha$ and $\Delta\delta$ are the angular deviations from beam center, and the beamwidths on the two axis of the ellipse are BW_α and BW_δ. Once the received power is obtained, the signal-to-noise ratio (SNR) is computed by means of

$$SNR = 10\log_{10}\frac{P_{Rx}}{k_B B_n T_0}, \quad [7]$$

in which k_B is the Boltzmann constant, B_n is the bandwidth of the receiver and T_0 is the noise temperature at the receiver. In Figure 5 the illuminated beams are plotted in the Hour Angle (HA) and declination (DECL) plane and colored according to their maximum value of SNR, normalized with respect to the maximum SNR among all beams. In this case the object transits really close to the central beam (nominal pointing of the Rx) and the corresponding color is therefore white. Non-illuminated beams are colored in black.

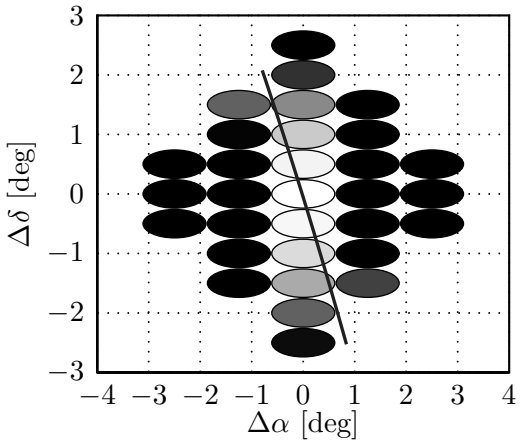

Figure 5: Example of SNR measure with the multibeam receiver. Maximum SNR ratio is obtained for each beam and normalized with the measured maximum SNR among all 31 beams.

The resulting simulated measures are organized in a text file, reporting the measured Δt,

*www.space-track.org

Δf, and SNR for each beam and for each time. The data are the input to the tailored orbit determination algorithms described in the following section.

IV ORBIT DETERMINATION PROCEDURE

The orbit determination phase is divided into two phases

1. Estimation of topocentric right ascension α and declination δ from SNR measures
2. Estimation of object position and velocity via batch least square optimization

The first step is tackled as a weighted curve fit. In most cases the relative motion of satellites and debris with respect to both receiver and target is fast enough to approximate the motion within the FOV of both radars as a straight line. As a consequence the "tracklet" inside the FOV of the receiver can be expressed as a function of time as

$$\begin{cases} \alpha(t) = a_1\, t + a_0 \\ \delta(t) = b_1\, t + b_0 \end{cases} \quad [8]$$

The coefficients a_1, a_0, b_1, and b_0 of Eq. [8] are estimated in two steps by using two different approaches. Thi first approach consist in a curve fit that minimizes the angular displacement from each beam center at the time of the maximum received power. The right ascension and declination of each beam are indeed known from the radar pointing (azimuth and elevation) and the time at which the maximum SNR occurs can be determined from the simulated measures. The selected weights are the normalized values of the SNR: the more the value of the weight is closer to one (maximum measured SNR among all beams) the more the object was closer to the beam axis.

The estimation of the right ascension and declination of the observed object is subsequently refined by taking into account the observation geometry, represented in Figure 6.

A North-West-Zenith (NWZ) topocentric reference frame is placed on the receiver (9). The azimuth and elevation of the transmitter Az_{Tx} and El_{Tx} can be computed since its location is known. When the information on azimuth

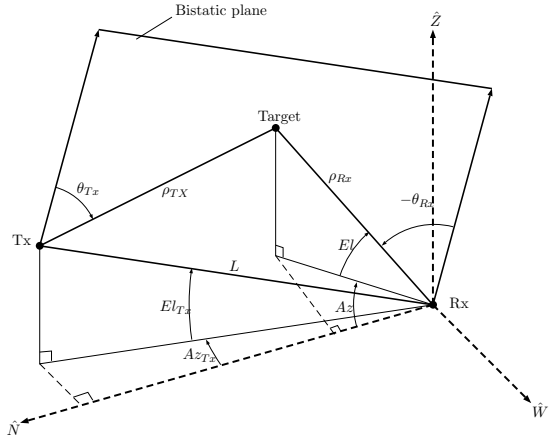

Figure 6: General geometry of bistatic plane with respect to NWZ frame, centered at the receiver.

Az and elevation El of the observed object are known it is possible to compute the angle θ_{Rx} on the bistatic plane as

$$\theta_{Rx} = -\arcsin\left[\cos El \cos El_{Tx} \cos(Az - Az_{Tx}) + \sin El \sin El_{Tx}\right] \quad [9]$$

Once θ_{Rx} is available the range between the receiver and the target is computed by means of

$$\rho_{Rx} = \frac{c\Delta T - L^2}{2\left(c\Delta T + L \sin\theta_{Rx}\right)} \quad [10]$$

and the range from transmitter to target is subsequently obtained as

$$\rho_{Tx} = \sqrt{\rho_{Rx}^2 + L^2 + 2L\rho_{Rx}\sin\theta_{Rx}} \quad [11]$$

The information on the range and Tx and Rx beams nominal directions can be used to estimate the SNR by means of Eqs. [5] and [7]. This allows to perform another fitting of the right ascension and elevation to reproduce the beam illumination sequence for all measured times.

In Figure 7 an example of the right ascension α and declination δ estimation phase is given. It can be observed how the second fit (red line) allows to get closer to the true trajectory, with an accuracy below the size of the beams.

Once the information on right ascension and declination are obtained, a batch least square optimization is performed taking into account also

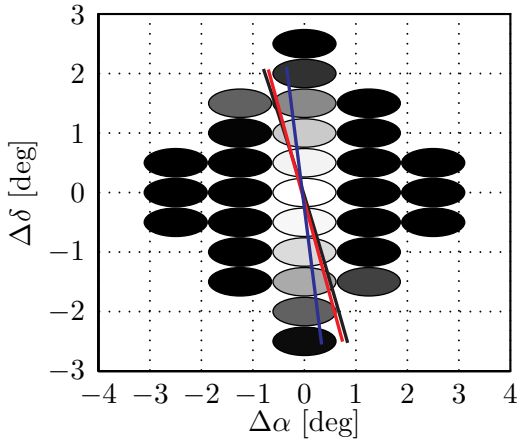

Figure 7: Determination of right ascension and declination from measured data. Black line is the true trajectory, blue line is the first guess obtained with the fit of the maximum SNR, and red line is the refined trajectory in the $\alpha - \delta$ plane.

Doppler shift and time delay. A first guess of the initial orbital state is obtained from TLE at the beginning of the observation and the trajectory is propagated for the duration of the satellite transit through the FOV of the instrument. Residuals are computed taking into account the bistatic range, the sum of the radial velocities from Tx and Rx, and the right ascension and declination at each time step. At each iteration an approximate solution of a linear system with the preconditioned conjugate gradient is performed and the procedure is stopped when the change in the objective function or orbital state is below the desired tolerance. At the last step both residuals $\boldsymbol{h}$ and Jacobian $\boldsymbol{J}$ are available and can be used to estimate the covariance matrix $\boldsymbol{C}$ resulting from the OD process by

$$\boldsymbol{C} = \frac{1}{N-n}\,\boldsymbol{h}^T\boldsymbol{h}\left(\boldsymbol{J}^T\boldsymbol{J}\right)^{-1}, \qquad [12]$$

where N is the length of the vector of residual and n is the number of variables, that in this case are the six orbital elements.

V NUMERICAL RESULTS

In the following the results of the orbit determination process for three different radar observations are considered. The first radar observation is performed by considering as a transmitter the antenna located in Bagnara. The remaining observations regard the same object transit but the transmitter in Bagnara and near SRT are used for the second and third observation respectively.

The transit time on the local meridian of the Northern Cross and azimuth and elevation of both TX and RX are given in Table 2. The pointing of the antennas are obtained from the most recent TLE released before the selected transit.

The resulting radar tracklet inside the receiver field of view for the first test case is represented in Figure 8. In this case 31 beams are formed inside the antenna FOV. Each beam is colored using a greyscale according to the maximum receiver power and the estimated trajectory in the right ascension/declination plane is represented as a red line. The reference trajectory, used to generate the simulated data, is the black line.

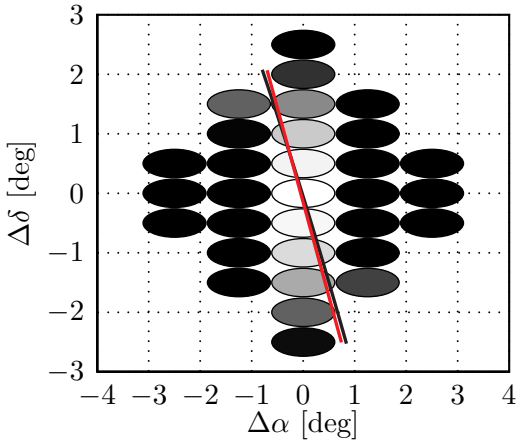

Figure 8: Receiver tracklet for observation 1. Red line is the estimated $\alpha-\delta$ trajectory whereas black line is the true trajectory.

The estimated orbital state and standard deviations for each state component are given in Table 3, together with the reference orbital state. The reference epoch for the state is equal to the time at which the first echo from the object is detected by the receiver. It can be observed that the standard deviations are of the order of a few tens of meters for all components and uncertainty on velocity is of the order of a few m/s. The reference state is comprised in the $\pm 3\sigma$ interval and is thus compatible with the estimated state.

The estimated orbital parameters are propa-

gated for the 24h following the observation to compare the error on position and velocity with respect to the reference trajectory. The goal of this analysis is to understand wether additional measures could be performed with the available information. The position and velocity errors are plotted in Figure 9. The orbital propagation are performed with the numerical propagator AIDA and information on the ballistic coefficient and SRP area are estimated from available TLEs of the object. It can be observed that the error on position remains below 35 km and it could be theoretically possible to perform additional observations of the object using the estimated orbital parameters.

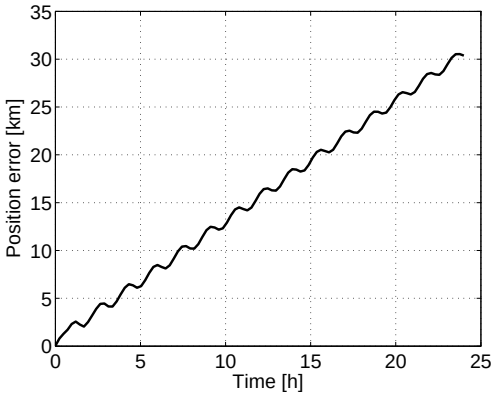

(a) Position error

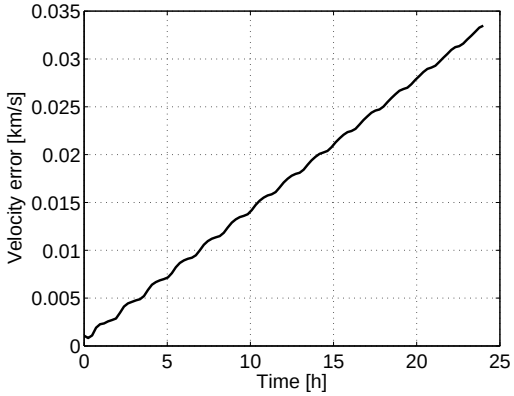

(b) Velocity error

Figure 9: Position and velocity error between reference and estimated trajectory for 24 h after OD.

The data acquisition for the transit of object 37820 is simulated by considering both transmitters location, resulting in observation 2 and 3 respectively. The resulting radar tracklets inside the receiver field of view are represented in Figure 8. In this case 32 beams are formed inside the antenna FOV. Since the azimuth and elevation of the receiver are the same for both observations, the resulting tracklets are the same.

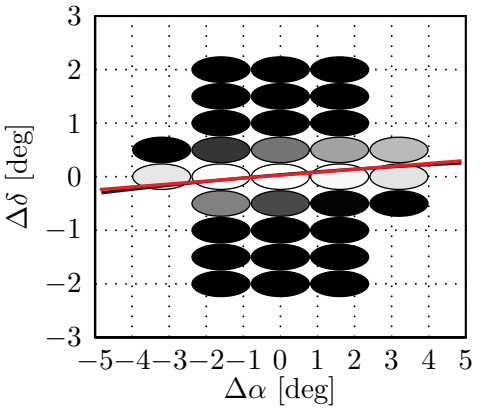

(a) Receiver tracklet for observation 2.

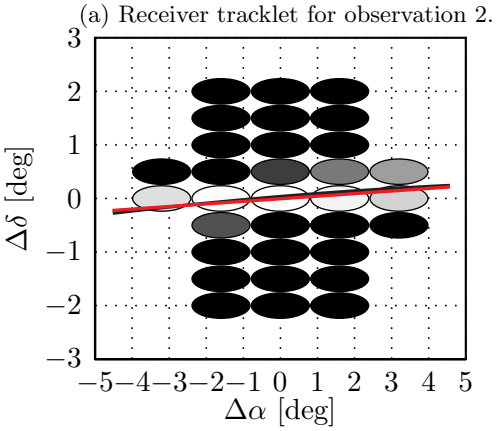

(b) Receiver tracklet for observation 3.

Figure 10: Radar tracklets for observation 2 and 3. Red line is the estimated $\alpha - \delta$ trajectory whereas black line is the true trajectory.

For each of the two observations the orbit determination is performed independently, i.e. without using the simulated data from the other. The resulting orbital state are listed in Table 4. Again the reference epoch is the time at which the first echo is measured by the receiver. As a result, the case with a lower slant range has a reference epoch that is 0.30 s earlier than the other. For both cases the standard deviations of the estimated orbital states are larger than the one obtained for observation 1. In particular, the configuration with the receiver located

near SRT has higher uncertainties. With respect to the previous orbit determination the difference between the reference and estimated state is larger. A possible reason could be the different beam configuration that is not symmetric in this case, coupled with the trajectory on the $\alpha - \delta$ plane, that is mainly horizontal and covers mainly one row of beams.

VI CONCLUSIONS

A method for the orbit determination of space debris using data from a bistatic radar system with a multibeaming receiver is presented. To test the effectiveness of the proposed method a simulator was developed to produce observation data. Given location and pointing angles for transmitter and receiver, as well as antenna characteristics, the power at the receiver, doppler shift, and time delay are computed for any object that transits within the volume defined by the intersection of the two beams. The simulator also allows to test different beamforming geometries for the receiver, using different sizes and locations for each beam.

Numerical tests of the OD algorithms were performed using simulated data. The method was able to retrieve an orbital state in all cases with just a single pass. For the first case the estimated and reference orbital state were compatible and standar deviations on position were on the order of a few tens of meters. For the other test cases sightly larger uncertainties were obtained although the error with respect to the reference values was larger.

This preliminary analysis and results will be extended in future works. Different solutions for the transmitting antenna will be tested together with different locations for the transmitter. In addition, different beamforming geometry will be tested to support the possible upgrade strategies for the Northern Cross, taking into account the complete refurbishment of the antenna. The large area of approximately 31,000 sqm could provide a high sensitivity and the maximum FOV of 120 sq. deg. could be "plastered" with up to 46,000 beams 4'×4' wide. Tests on this configuration will be performed to assess the improvements in the accuracy of the orbit determination process and possibly determining wether a real-time OD process can be performed.

REFERENCES

(1) T. Flohrer, H. Krag, S. Lemmens, B. Bastida Virgili, K. Merz, and H. Klinkrad. Statistical Look on ESA's Conjunction Event Predictions. *Proc. of the 6th Europ. Conf. on Space Debris, Darmstadt, Germany*, ESA SP-723, 2013.

(2) M. J. Matney and E. Stansbery. What are radar observations telling us about the low-Earth orbital debris environment? In *Space Debris*, volume 473 of *ESA Special Publication*, pages 43–48, October 2001.

(3) D. Mehrholz, L. Leushacke, and D. Banka. Beam-park experiments at FGAN. *Advances in Space Research*, 34(5):863 – 871, 2004.

(4) J Markkanen. Space debris measurements with EISCAT radars-the first 1000 hours. In *36th COSPAR Scientific Assembly*, volume 36, page 2934, 2006.

(5) E.F. Knott, M.T. Tuley, and J.F. Shaeffer. *Radar Cross Section*. Scitech Publishing, 2004.

(6) S. Montebugnoli, G. Bianchi, J. Monari, G. Naldi, F. Perini, and M. Schiaffino. BEST: Basic Element for SKA Training Wide Field Science and Technology for the Square Kilometre Array. In *Proceedings of the SKADS Conference*, pages 331–336, Château de Limelette, Belgium, November 2009.

(7) G. Foster, J. Hickish, A. Magro, D. Price, and K. Zarb Adami. Implementation of a direct-imaging and fx correlator for the best-2 array. *Monthly Notices of the Royal Astronomical Society*, 439(3):3180–3188, 2014.

(8) A. Magro, J. Hickish, and K. Zarb-Adami. Mulitbeam GPU Transient Pipeline for the Medicina BEST-2 Array. *Journal of Astronomical Instrumentation*, 2(1), 2013.

(9) Nicholas J Willis. *Bistatic radar*. SciTech Publishing, 2005.

Table 2: Time of observation and antenna pointing

Obs.	**Transit epoch**	**Object ID**	**RX**	**Az [deg]**	**El [deg]**	**TX**	**Az [deg]**	**El [deg]**
1	2014/07/01 19:52:15	19046	NC	0.0	86.2	Bagnara	343.4	84.3
2	2014/04/15 13:22:36	37820	NC	180.0	61.6	Bagnara	184.9	63.5
3	2014/04/15 13:22:36	37820	NC	180.0	61.6	SRT	27.8	41.6

Table 3: Estimated orbital state and 1σ standard deviations for observation 1. Reference epoch for observation is 2014/01/07 19:52:11.85 UTC.

	RX [km]	**RY [km]**	**RZ [km]**	**VX [km/s]**	**VY [km/s]**	**VZ [km/s]**
Ref. state	-3209.7092	-3748.5452	4849.5759	2.34464	4.90000	5.32039
Est. state	-3209.7443	-3748.5092	4849.5830	2.34557	4.89947	5.32026
St. dev. σ	$\pm$0.0140	$\pm$0.0159	$\pm$0.0216	$\pm$0.00161	$\pm$0.00107	$\pm$0.00055

Table 4: Estimated orbital state and 1σ standard deviations for observation 2 and 3.

	RX [km]	**RY [km]**	**RZ [km]**	**VX [km/s]**	**VY [km/s]**	**VZ [km/s]**
Observation 2, reference epoch: 2014/04/15 13:22:31.85 UTC						
Ref. state	2829.9538	4081.4808	4562.3438	-6.50287	4.07853	0.38943
Est. state	2829.9115	4081.3228	4562.4820	-6.50102	4.08466	0.37211
St. dev. σ	$\pm$0.0265	$\pm$0.0351	$\pm$0.0166	$\pm$0.00061	$\pm$0.00069	$\pm$0.00201
Observation 3, reference epoch: 2014/04/15 13:22:32.15 UTC						
Ref. state	2828.0027	4082.7042	4562.4603	-6.50397	4.07695	0.38765
Est. state	2827.8382	4082.3742	4562.4815	-6.49579	4.08926	3.75411
St. dev. σ	$\pm$0.0353	$\pm$0.0480	$\pm$0.0186	$\pm$0.00135	$\pm$0.00156	$\pm$0.00165